ACS APPLIED MATERIALS & INTERFACES

Research Article

www.acsami.org

Graphene Oxide-Immobilized NH_2-Terminated Silicon Nanoparticles by Cross-Linked Interactions for Highly Stable Silicon Negative Electrodes

Cheng Sun,[†] Yuanfu Deng,*[,‡,§] Lina Wan,[‡] Xusong Qin,[§,∇] and Guohua Chen*[,†,§,∇]

[†]Fok Ying Tung Graduate School, The Hong Kong University of Science and Technology, Clear Water Bay, Kowloon, Hong Kong, China

[‡]The Key Laboratory of Fuel Cell for Guangdong Province, School of Chemistry and Chemical Engineering, South China University of Technology, Guangzhou, China

[§]Center for Green Products and Processing Technologies, Guangzhou HKUST Fok Ying Tung Research Institute, Guangzhou 511458, China

[∇]Department of Chemical and Bioolecular Engineering, The Hong Kong University of Science and Technology, Clear Water Bay, Kowloon, Hong Kong, China

Supporting Information

ABSTRACT: There is a great interest in the utilization of silicon-based anodes for lithium-ion batteries. However, its poor cycling stability, which is caused by a dramatic volume change during lithium-ion intercalation, and intrinsic low electric conductivity hamper its industrial applications. A facile strategy is reported here to fabricate graphene oxide-immobilized NH_2-terminated silicon nanoparticles (NPs) negative electrode (Si@NH_2/GO) directed by hydrogen bonding and cross-linked interactions to enhance the capacity retention of the anode. The NH_2-modified Si NPs first form strong hydrogen bonds and covalent bonds with GO. The Si@NH_2/GO composite further forms hydrogen bonds and covalent bonds with sodium alginate, which acts as a binder, to yield a stable composite negative electrode. These two chemical cross-linked/hydrogen bonding interactions—one between NH_2-modified Si NPs and GO, and another between the GO and sodium alginate—along with highly mechanically flexible graphene oxide, produced a robust network in the negative electrode system to stabilize the electrode during discharge and charge cycles. The as-prepared Si@NH_2/GO electrode exhibits an outstanding capacity retention capability and good rate performance, delivering a reversible capacity of 1000 mAh g^{-1} after 400 cycles at a current of 420 mA g^{-1} with almost 100% capacity retention. The results indicated the importance of system-level strategy for fabricating stable electrodes with improved electrochemical performance.

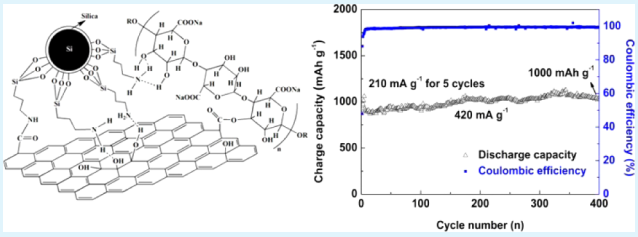

KEYWORDS: *Si-based anode, graphene oxide, Li-ion batteries, cycling stability, cross-linking*

INTRODUCTION

Developing lithium-ion batteries (LIBs) with high energy, power density, and long cycle life is of key importance to meet the ever-increasing energy storage needs for various applications such as portable electronic devices, hybrid electric vehicles (HEVs), pure electric vehicles (EVs), and even grid-scale energy storage systems.[1−3] Battery performance depends critically on the electrode materials; therefore, the development of new materials is very important. Graphite, which is the most common anode material for current commercial LIBs, cannot fulfill the requirement of high-energy applications, because of its limited specific capacity, with a theoretical value of 372 mAh g^{-1}.[4] Different types of anode materials with high specific capacities have been proposed for LIBs. Among them, silicon (Si) has attracted great attention, because of its high specific capacity (~4000 mAh g^{-1}), low lithium discharge potential (~0.5 V vs Li/Li^+), and environmental benignity.[5−7] However, the practical application of micrometer-sized bulk Si-based electrode materials is still hampered by its low electric conductivity and large volume change (~400%) during the discharge and charge processes, resulting in fracture, pulverization, and final loss of electric contact from the current collector, which all lead to low rate performance and fast capacity fade upon cycling.[8] It is commonly acknowledged that nanostructured Si can partially overcome the aforementioned limits. Nanostructured Si is more resistant to mechanical strain during lithium-ion insertion/desertion than bulk one and could provide shorter path length for the transport of electron and lithium ion and improve conductivity as well as charge/discharge rate.[7] As a result, significant progress has been made

Received: March 17, 2014
Accepted: June 12, 2014
Published: June 12, 2014

on developing Si in the forms of nanowires,[9] nanotubes,[10] nanospheres,[11] and nanofibers.[12] Nevertheless, synthesizing Si with special nanostructures usually involves a complex chemical route and high-temperature processes such as chemical vapor deposition, which is expensive and difficult to scale up.[12] Developing Si-based nanomaterials with stable electrochemical performance through relatively facile processes is still very important and challenging.

Recently, the utilization of carbon materials in making Si nanoparticles composites as anode materials for LIBs has become another effective strategy to address the low rate and poor cycle performance problems of Si nanoparticles (NPs).[13−26] A key role of carbon materials in those types of Si-based anode nanostructures is that they can buffer the pulverization of Si upon lithiation. Among these composites with carbon and various morphologies of Si nanomaterials, reduced graphene oxide (RGO)/Si NPs hybrid materials have shown promising electrochemical performance, because RGO has superior electrical conductivity, high surface area (2600 $m^2 g^{-1}$), excellent chemical stability, and strong mechanical strength.[18−26] Besides the composite materials, electrodes made from Si NPs using special polymer binders, such as polyacrylic acid (PAA),[15,27] carboxyl-methyl cellulose (CMC),[28,29] alginate (Alg),[30] CMC and PAA composite binder,[31] or mussel-inspired adhesive binders (dopamine)[32] have been found to have good cycle stability in more recent years. The cycle life improvement by using PAA, CMC, and Alg binders was attributed to the binding interaction between the functional groups on the polymers and the surface oxide on Si NPs. According to the above-mentioned strategies, it is clear that most of the research on the Si-based anode materials has been focused on either designing Si-based novel nanostructures or manufacturing the stable electrodes using novel binders. However, such investigations of active materials or binders have not provided sufficient solutions to the technological challenges for the development of the modern battery industry. It may be helpful to pay attention to the development of the electrode system as a whole. It is expected that further improvement of the cycle life and rate performance of Si-based anode materials can be realized by optimizing the complete system and studying the interactions between these individual components.

In this paper, a novel strategy for constructing enhanced interfacial bonding for silicon-based anodes is reported for energy storage. Specifically, a NH_2-terminated Si/GO (Si@NH_2/GO) composite was fabricated. GO was selected as a substrate to anchor the Si@NH_2, because it can increase the chemical interaction via cross-linking reaction derived from both the high surface area and the rich functional groups on its surface. RGO, which has been extensively studied as a component for composite materials previously,[13−26] was not adopted, because of the insufficient number of functional groups on its surface. The fabrication of the composite materials involves a two-step design to build three stable interfaces between Si NPs and aminopropyltriethoxysilane (APTES), APTES and GO, and GO and binder. The as-obtained electrode exhibited much improved cycling performance and good rate capability, which made it an effective strategy to design a novel Si-based electrode with good performance.

EXPERIMENTAL SECTION

Si NPs were purchased from Alfa Aesar. Aminopropyltriethoxysilane (APTES) and other reagents were purchased from Aladdin. All reagents were used as received without further purification. The Si NPs were first treated by HCl solution to obtained OH-terminated Si (Si@OH) NPs. Then, the Si@OH NPs were NH_2-terminated via the surface grafting of APTES in toluene solution.[33,34] The APTES on the Si surface can function as a buffer, and it also can provide a positively charged surface to realize the self-assembling of Si and the negatively charged graphene oxide (GO)[35] by hydrogen bonding interaction.[20,21,24,25] A cross-linking reaction then happened between the buffer and GO by thermal treatment in Ar. After the Si@NH_2/GO nanocomposite was mixed with sodium alginate (Salg) binder in water, another chemical binding reaction between GO and binder would take place through thermal treating the mixture on the current collector in a vacuum. In addition, this low-temperature heat treatment process can partially remove and/or chemically modify some of the functional groups on the GO surface and improve the electronic conductivity[36] of the as-prepared Si@NH_2/GO nanocomposite.

Preparation of NH_2-Terminated Si Nanoparticles (Si@NH_2 NPs)..[33,34] In a typical experiment, the pursued Si NPs were immersed in hydrochloride solution (37%) for 1 h at room temperature with high-speed stirring. Thereafter, the product was filtered, washed by deionized water three times, and dried under vacuum at 80 °C for 2 h to obtain the OH-terminated Si nanoparticles (Si@OH NPs). Then, the Si@OH NPs (500 mg) were dispersed into 50 mL of dry toluene solution via sonication for 2 h. Afterward, 0.5 mL of APTES was poured in and the mixture was refluxed at 110 °C for 24 h under a nitrogen atmosphere. Subsequently, the product was filtered, washed by acetone three times, and dried under vacuum (0.01 MPa) at 60 °C overnight.

Preparation of the Si@NH_2/GO Composite. GO nanosheets were prepared from natural graphite using a modified Hummers' method.[37,38] The suspension of Si@NH_2 (1 mg mL^{-1}) in water was added dropwise into a diluted (GO) aqueous dispersion (1 mg mL^{-1}, pH 6.0) under fast stirring (400 rpm) for 2 h. The precipitate was filtered and washed by ethanol three times, followed by a thermal treatment at 150 °C in a furnace for 12 h under an Ar atmosphere.

Preparation of the Si@OH/GO Composite. Si@OH/GO composite was prepared using a procedure similar to that used for the preparation of Si-@NH_2/GO, except NH_2-terminated Si NPs were substituted with Si@OH NPs.

Physical Characterizations. Fourier transform infrared spectroscopy (FT-IR) spectra were documented with KBr pellets from a Bruker Model R 200-L spectrophotometer. Raman spectra were obtained with a Bio-Rad Model FTS6000 Raman spectra were obtained with a Bio-Rad FTS6000 Raman microscopy with a 532 nm blue laser beam. Thermogravimetric analyses (TGA) were conducted using a thermogravimetric analyzer (TA Instruments, Model TGA-Q50) in air at a scan rate of 5 °C min^{-1} from room temperature to 700 °C. The morphologies and crystalline structures of the obtained composite were characterized by scanning electron microscopy (SEM, JSM Model 6390) and transmission electron microscopy (TEM) (JEOL, Model 2010F). X-ray photoelectron spectroscopy (XPS) measurements were performed using a Kratos Axis Ultra spectrometer with focused monochromatic Al Kα radiation ($h\nu$ = 1486.6 eV).

Electrochemical Tests. All of the tests were performed with CR2025 coin half-cells. The Si-based negative electrodes were made from the mixtures of 60 wt % Si/GO composite, 20 wt % super P, 20 wt % sodium alginate (Salg) on copper foil, with an average composite loading of ~1.5 mg·cm^{-2}, and dried for 12 h at 100 °C under vacuum (1000 Pa). The electrodes were punched into disks with a diameter of 14 mm and pressed at 10 MPa thereafter. The electrolyte was composed of 1.0 M $LiPF_6$ in a mixture of ethylene carbonate (EC), dimethyl carbonate (DEC), and ethyl methyl carbonate (EMC) (1:1:1, v/v) with 3 wt % vinylidene carbonate (VC). Celgard 2400 was used as the separator. Cells were assembled in an Ar-filled glovebox (Master 100 Lab, Braun, Germany) with less than 1 ppm of both oxygen and moisture. The cells were electrochemically cycled between 0.01 and 1.0 V at different charge/discharge rates on a multichannel battery test system (Neware, Model CT-3008W). The specific capacity was calculated based on the mass of the Si@NH_2/GO composite. The cyclic voltammetric (CV) tests were carried out on an Electrochemical

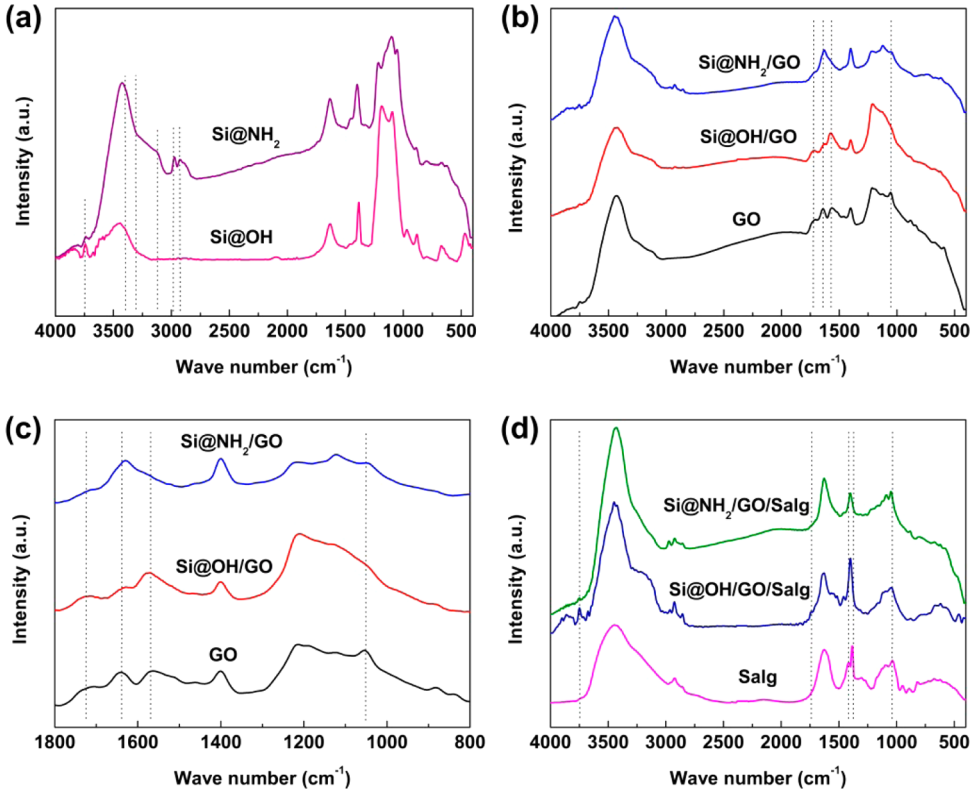

Figure 1. Fourier transform infrared (FT-IR) spectra of the obtained Si-based materials: (a) FT-IR spectra of the Si@OH and Si@NH_2; (b, c) FT-IR spectra of the GO, Si@OH/GO and Si@NH_2/GO composites (d) FT-IR spectra of the Salg, Si@OH/GO/Salg and Si@NH_2/GO/Salg electrodes.

Workstation (Autolab PGSTAT 101) at a scan rate of 0.1 mV s^{-1}. The electrochemical impedance spectroscopy (EIS) data of the electrodes were acquired at room temperature, using a Versa-stat 3 electrochemical workstation (Princeton Applied Research) after a desired number of cycles at a constant potential of ~1.0 V (vs Li/Li^+) in the frequency range from 100 kHz to 10 mHz by imposing an alternate current with an amplitude of 10 mV on the electrode.

RESULTS AND DISCUSSION

After treatment with hydrochloride, the Si NPs are oxidized to form a layer of silicon dioxide on their surface. It has been known that the Si@OH NPs are negatively charged, which is difficult to assemble with the negatively charged GO from the ionization of the carboxylic acid and phenolic hydroxyl.[19] However, the Si@OH NPs can be easily modified via the surface grafting of APTES via covalent bonds to make the surface positively charged in acid solution.[20,21] Therefore, the surface-modified Si NPs can be well dispersed on GO through hybrid electrostatic/hydrogen-bonding self-assembly. To obtain cross-linking reaction between the $-NH_2$ groups on the Si@NH_2 and the carboxylic groups on the GO, the obtained Si@NH_2/GO composite was thermally treated at 150 °C in an Ar atmosphere.[39]

Figure 1 shows the FTIR spectra of the Si-based materials obtained from different treatment processes for Si NPs. In the spectrum of the initial Si@OH (Figure 1a), the peak at 3739 cm^{-1} is assigned to the stretching of free silanol group.[34] The Si−OH groups and H_2O molecules absorbed on the surface display a band at 1630 cm^{-1}. Comparing with the IR spectrum of Si@OH, there are two peaks at ~2970 and 2930 cm^{-1} in the Si@NH_2 spectrum, which are assigned to the vibrations of methyl/methylene in the APTES molecule.[24,25] The typical bands of ~3350, 3300, and 3100 cm^{-1} are assigned to the asymmetric $-NH_2$ stretch, the symmetric $-NH_2$ stretch, and deformation of the hydrogen-bonded amino group, respectively.[40] In addition, the peak at 3739 cm^{-1} in the Si@NH_2 spectrum is much weaker than that in the Si@OH spectrum. These observations suggest that APTES have been grafted successfully onto the Si@OH NPs via covalent bonds. A typical broad peak is observed in the range between 3300 cm^{-1} and 3100 cm^{-1} in the Si@NH_2 sample, which is assigned to some hydrogen-bonding interactions between partial NH_2 groups of APTES and hydroxyl groups on the surface of Si NPs. For GO, the presence of the two peaks at 1715 and 1050 cm^{-1}, corresponding to the stretching vibration of C═O for −COOH and C−O for C−OH, respectively, demonstrates that there are carboxylic and hydroxyl groups in GO (Figure 1b).[41] After Si@NH_2/GO composite formation via the thermal treatment, the relative intensity of 1715 cm^{-1} decreased significantly and the peaks of 1635 and 1553 cm^{-1} disappeared with a new peak forming at 1628 cm^{-1} instead, which is attributed to the C═O stretching vibration of amide (Figure 1c). This result provides a proof of the occurrence of chemical cross-linking reaction/strong hydrogen-bonding interaction between the Si@NH_2 and GO.[39] For Si@OH/GO composite, the relative intensity of 1715 cm^{-1} does not change significantly, compared with that of GO, indicating no obvious chemical cross-linking reaction between the −COOH of GO and hydroxyl groups of Si@OH (Figure 1c). However, the relative intensity of ~3200 cm^{-1} does increase and the peak of ~1080 cm^{-1} decreased significantly, which might be attributed to some hydrogen-bonding interactions between the hydroxyl groups on the Si@OH NPs and the functional groups on GO. To achieve cross-linking reaction between GO and Salg, the working electrode containing Si@NH_2/GO composite, super P,

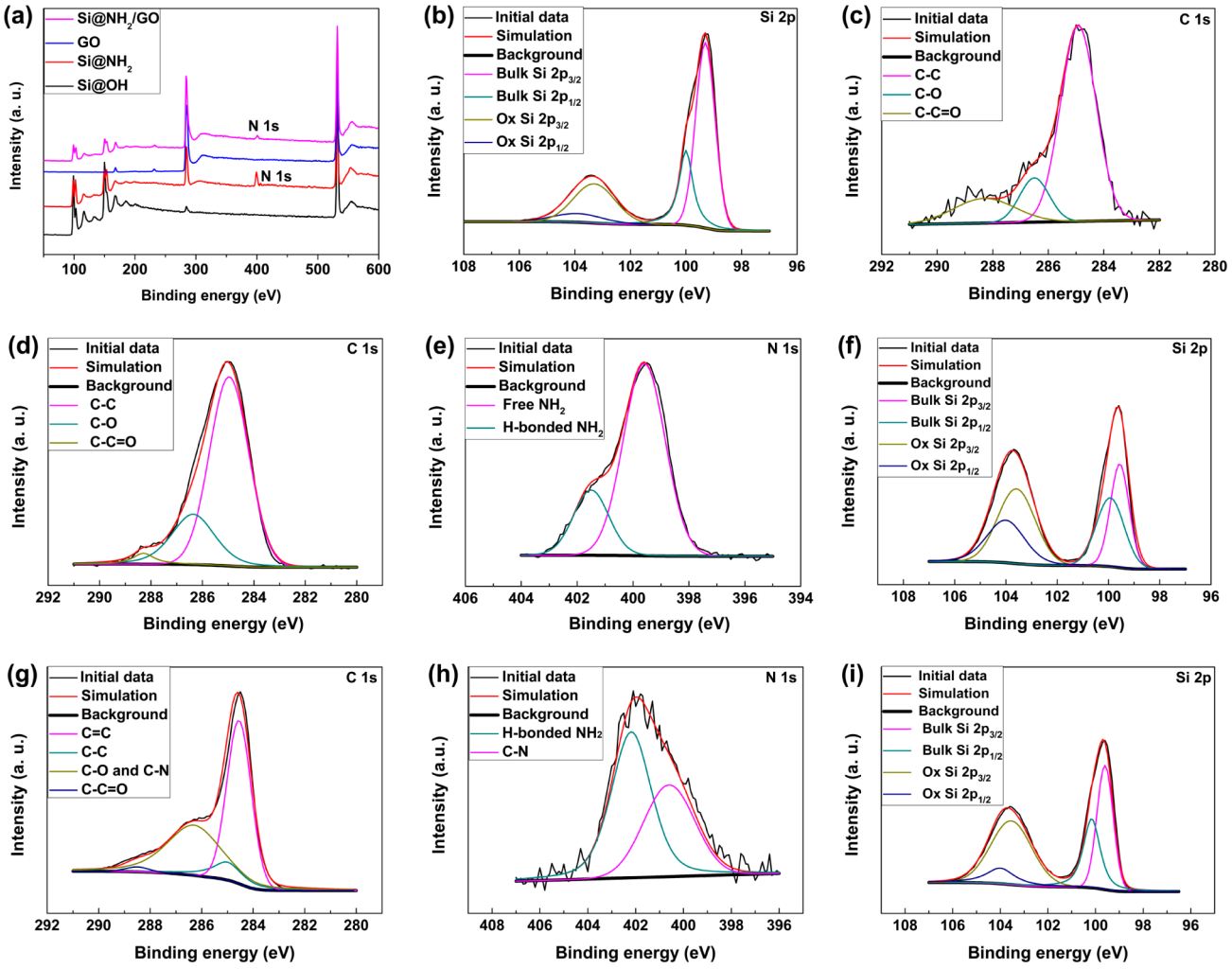

Figure 2. XPS of the different Si-based materials obtained from different treatment of Si NPs: (a) XPS spectra of the obtained Si@OH, Si@NH_2, GO, and Si@NH_2/GO samples; (b) Si 2p spectrum of Si@OH; (c) C 1s spectrum of Si@OH; (d) C 1s spectrum of Si@NH_2; (e) N 1s spectrum of Si@NH_2; (f) Si 2p spectrum of Si@NH_2; (g) C 1s spectrum of Si@NH_2/GO; (h) N 1s spectrum of Si@NH_2/GO; and (i) Si 2p spectrum of Si@NH_2/GO.

and Salg pasted on copper foil was treated at 150 °C under vacuum (1000 Pa). As shown in Figure 1d, the weak peak at 1715 cm^{-1} of Si@NH_2/GO composite, which is attributed to the chemically cross-linked reaction between the partially functional groups of GO and the binder, disappeared after it was treated with Salg at 150 °C overnight. At the same time, the typically broad peak ranging from 3300 cm^{-1} to 3100 cm^{-1} in the thermally treated electrode became weaker, compared to the Si@NH_2/GO composite. It can be therefore concluded that a covalent bond has been formed between GO and Salg during the vacuum-drying process. As to Si@OH/GO with Salg, a small peak at 1715 cm^{-1}, attributed to the C═O stretching vibration of C═O for the −COOH group, is observed, which could be attributed to the surplus −COOH groups of GO after the chemical cross-link reaction between GO and Salg. The peak at ∼3500 cm^{-1}, which appear in all of the spectra (as shown in Figure 1d), should be attributed to the vibration of the absorbed water molecules.

There is not significant difference between the Raman spectra of Si@NH_2/GO and Si@OH/GO composites (see Figure S1 in the Supporting Information). Two peaks at 1350 and 1590 cm^{-1} correspond to the D and G bands of GO/graphene, respectively.[42] The compositions of Si@OH/GO and Si@NH_2/GO samples were also determined using TGA (see Figure S2 in the Supporting Information). The 5% mass loss below 150 °C corresponds to the loss of the absorbed water molecules on the surface of the three samples. A mass loss of 33% was observed between 200 °C and 500 °C for Si@OH/GO, which corresponds to the oxidation of GO in this sample. For the Si@NH_2/GO sample, a 35.5% mass loss between 200 °C and 500 °C corresponds to the oxidation of GO and the APTES molecule. For both Si@OH/GO and Si@NH_2/GO samples, the Si nanoparticles are stable up to 550 °C.[24] The gradual increase in mass above 550 °C is attributed to oxidation of the Si core. Based on the above analysis, the overall mass percentages of Si in the Si@OH/GO and Si@NH_2/GO samples are 70.5% and 67.8%, respectively.

X-ray photoelectron spectroscopy (XPS) analysis was conducted to monitor each step of the Si@NH_2/GO composite preparation. Figure 2a shows the entire XPS spectra of the obtained Si@OH, Si@NH_2, GO and Si@NH_2/GO samples. As shown in Figure 2b, two distinct doublets, corresponding to bulk silicon (98.7 eV) and silicon bonded to oxygen (103.1 eV), are observed.[43] Quantification of the high-resolution spectrum shows that the contributions of these two components in the Si@OH sample are 71% and 29%,

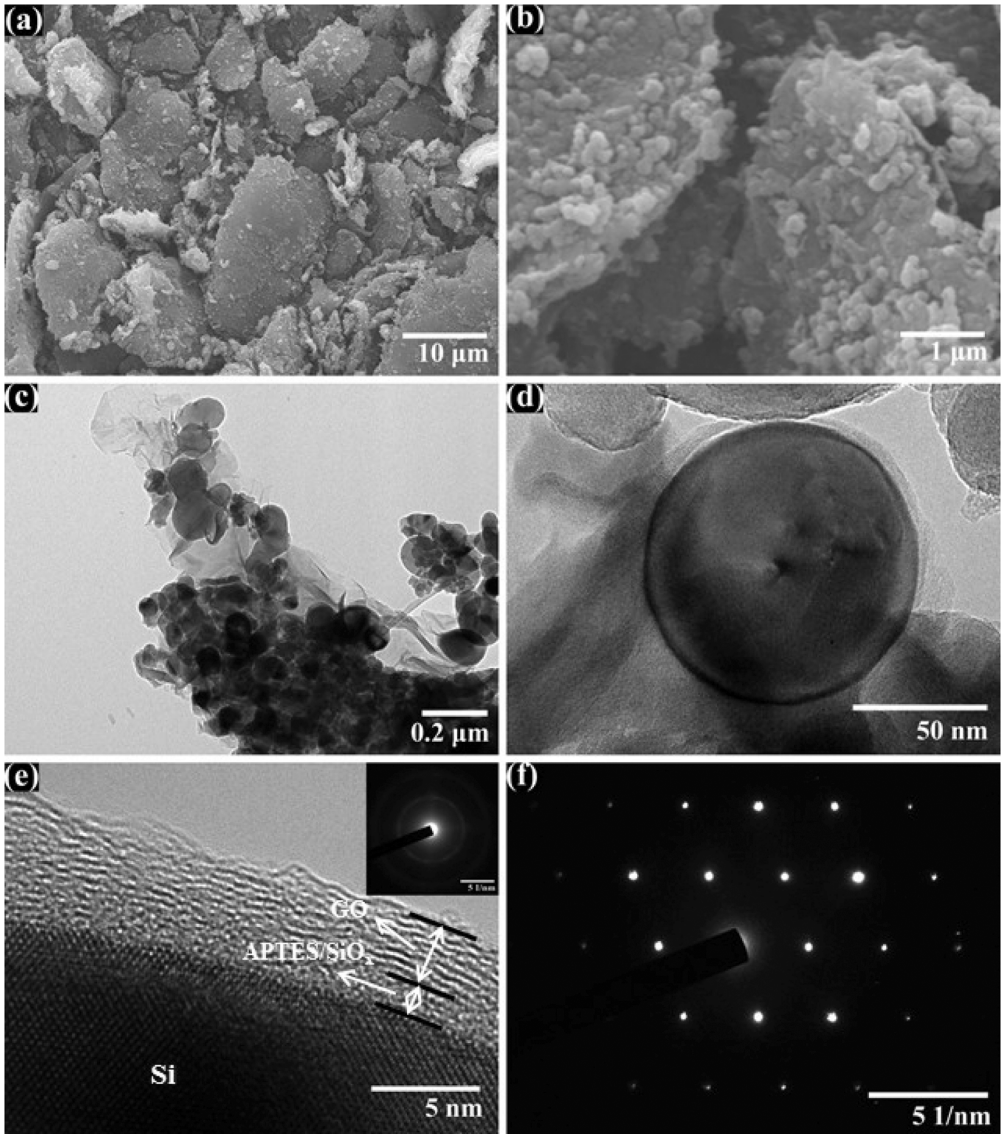

Figure 3. (a, b) SEM images of the Si@NH_2/GO composite; (c, d) TEM images of the Si@NH_2/GO composite; (e) HTEM image of the Si@NH_2/GO composite; and (f) electron diffraction pattern of the Si@NH_2/GO composite.

respectively. Observation of the C 1s spectrum in the Si@OH indicates the presence of hydrocarbon contamination on the surface (Figure 2c).[33] After surface modification by APTES, the C 1s spectrum (Figure 2d) shows all the expected functionality from APTES, namely, C−C at 285.0 eV, C−O/C−N at 286.4 eV, and C−C═O at 288.3 eV.[44] However, it is not significantly different from that of the Si@OH NPs, since hydrocarbon contamination also exhibits these functional groups. This phenomenon is similar to the previously reported results.[33] The presence of APTES on the surface can be confirmed by the N 1s spectrum (shown in Figure 2e). The peak at 401.5 and 399.6 eV are attributed to hydrogen-bonded NH_2 and free NH_2 of the APTES molecules, respectively.[45] These components are expected to be present in the spectrum of a surface that has been successfully modified with APTES. In addition, comparison between the Si 2p spectrum from the Si@NH_2 surface (Figure 2f) and that from Si@OH surface (Figure 2b) reveals that there is an increase in the Si−O peak (103.6 eV) from the bulk Si peak (99.6 eV). Such an increase on the Si@NH_2 surface may be resulted from two factors:[34] first, the APTES itself contains Si−O bonds, and, second, the APTES on the surface results in a thicker layer on top of the bulk silicon than the Si@OH alone, and this will, in turn, lead to an attenuation of the bulk Si XPS signal due to the limited probe depth of XPS. When the Si@NH_2 NPs are composited with GO, the C 1s signals are shifted to lower binding energy and their full width at half-maximum (fwhm) became narrower (Figure 2g), which are attributed to an enhanced degree of graphitization caused by the GO.[46] The obvious peak at 399.6 eV, corresponding to the free NH_2 of APTES in Si@NH_2, disappeared and two new peaks at 402.2 and 400.6 eV can be observed (Figure 2h), which are assigned to the strong hydrogen-bonded NH_2 and N 1s spectrum of amide, respectively.[46] This result provides a good case for the occurrence of chemical interaction between the Si@NH_2 and GO. Comparison between the N 1s spectrum from Si@NH_2/GO composite surface with the N 1s spectrum from Si@NH_2 shows that there is a decrease in the peak intensity, which is resulted from an additional GO layer on the surface of Si@NH_2. A similar decrease in the peak intensity of Si 2p can also be observed.

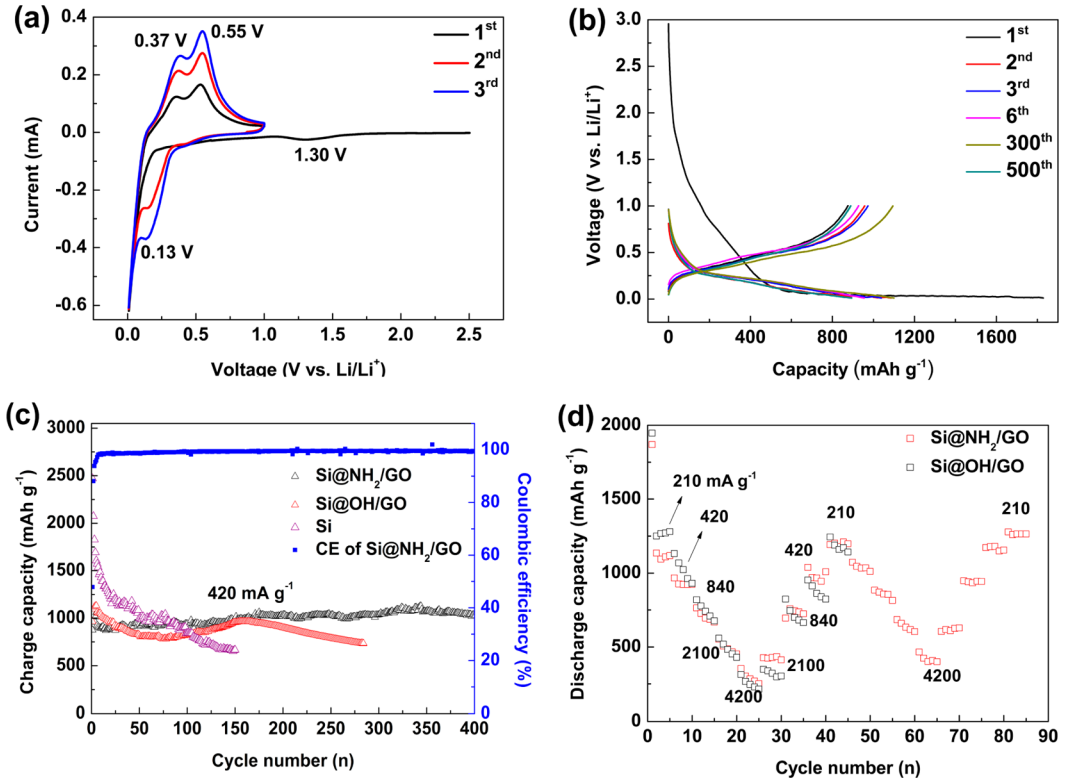

Figure 4. (a) CV curves of the first three cycles of the Si@NH_2/GO composite, (b) galvanostatic discharge and charge profiles of Si@NH_2/GO composite at different cycles, (c) cycling performance of Si@NH_2/GO, Si@OH/GO composites and pure Si nanoparticles, and (d) rate performance of Si@NH_2/GO and Si@OH/GO composites.

The morphology of the resulting Si@NH_2/GO composite is shown in Figure 3. The SEM image displays that this composite is a micrometer-sized nanocomposite with a rough and wrinkled surface (Figure 3a). In the high-magnification SEM image (Figure 3b), it is easy to see that the Si@NH_2 NPs are well-coated/immobilized by GO. The TEM image shows that the micrometer composite is composed of Si NPs and GO nanosheets (Figure 3c). The uniformly dispersed Si NPs are well-coated by GO sheets with wrinkles around the Si NPs. In addition, the HRTEM image reveals that a Si nanoparticle of ~100 nm in size, with a crystal structure and a thin coating on its surface, is well-coated by GO sheets with a thickness of several nanometers (Figures 3d and 3e). The ringlike mode in the selected-area electron diffraction (SAED) pattern (inset of Figure 3e) confirms the polycrystalline GO. The single crystal structure of Si is demonstrated by its separately single point in SAED (Figure 3f).

The characterization data obtained from FT-IR spectroscopy, Raman spectroscopy, SEM, TEM, HRTEM, and XPS analysis confirm that the Si nanoparticles in the Si@NH_2/GO nanocomposite have been satisfactorily modified by APTES molecules and the Si@NH_2 NPs have been well-immobilized by GO via chemical cross-linking/hydrogen-bonding interactions. Furthermore, the Si@NH_2/GO composite has also been well-immobilized with the binder (Salg) via chemical cross-linking reaction when it is used as an active material for a Si-based electrode. Such a composite is expected to have enhanced electrochemical performance when it is employed as anode material, as is indeed observed subsequently.

Figure 4a shows typical cyclic voltammetry (CV) curves of the Si@NH_2/GO nanocomposite electrode in the potential window of the open circuit voltage to 0.01 V of the first cycle and 1.0 to 0.01 V of the following two cycles at a scan rate of 0.1 mV s^{-1}. The cathodic part of the first cycle displays a broad peak centered at 1.3 V, which may be attributed to the decompositions of electrolyte additive (VC). The decompositions of VC help to form a proper protective SEI film in an early stage of the first discharge, which further decreases electrochemical reduction of the main electrolyte components (no obvious reduction peak at 0.8 V was observed).[47,48] Below 0.25 V, a sharp reduction peak for insertion of Li^+ into Si NPs could be observed, and subsequently, the extraction process occurred at 0.34 and 0.54 V with a broad peak. These redox/oxidation peaks are attributed to the alloying/dealloying of Li with active Si NPs. In the following cycles, the cathodic peak at 0.13 V gradually evolved, corresponding to the formation of Li–Si alloy phase. The anodic parts show two peaks at 0.37 and 0.55 V, which assigned to dealloying of Li–Si alloys. These results are consistent with the data previously reported for Si-based electrodes.[13,19,20]

Figure 4b displays the discharge–charge profiles of the first three cycles at a current density of 210 mA g^{-1} and the selective cycles at a current density of 420 mA g^{-1} between the voltage limits 0.01 and 1.0 V vs Li/Li^+. The specific discharge capacity is calculated using the total mass of Si@NH_2/GO composite. The initial discharge capacity is 1833 mAh g^{-1}, with a reversible charge capacity of 878 mAh g^{-1}. The large irreversible capacity of the Si@NH_2/GO composite can be attributed to the formation of SEI film and the lithium consumption of GO,[19,49] whose first specific discharge and charge capacities were 790 mAh g^{-1} and 100 mAh g^{-1}, respectively (see Figure S3 in the Supporting Information). The large irreversible capacity results in low Coulombic efficiency (CE) in the first cycle. In addition, the specific charge capacity in the initial several cycles shows an

activation process. After the activation process, the CE quickly reaches nearly 100% and remains relatively stable in subsequent cycles (Figure 4c). This high CE achieved here should be due in large part to the formation of a stable SEI on the composite electrode.

Figure 4c compares the long cyclic performance of the Si@NH_2/GO and Si@OH/GO composite-based electrodes at different current densities. The electrode made with the Si@NH_2/GO composite delivers a specific charge capacity of 1059 and 927 mAh g^{-1} at 210 and 420 mA g^{-1}, respectively. In the first several cycles, although the Si@OH/GO composite-based electrode displays higher specific capacities, compared to the Si@NH_2/GO composite-based electrode, the capacity declines very rapidly. After ~10 cycles, the specific capacity of the Si@NH_2/GO composite becomes higher than that of Si@OH/GO composite, showing its good capacity retention capability. This result demonstrates that the Si@OH/GO composite-based electrode may not maintain a stable SEI layer during the initial cycles. As shown in Figure 4c, the Si@NH_2/GO composite shows an excellent cycle performance. After 400 cycles, the reversible specific capacity for this composite is still as high as 1000 mAh g^{-1} (~1520 mAh g^{-1} based on the pure Si) with 100% capacity retention. It is noted that the capacity gradually increases during 400 cycles, which may be attributed to the interfacial lithium storage and the activation Si in the core upon cycling. Similar experimental results were also observed in Si-based[26] and other anode materials.[50] In contrast, the Si@OH/GO composite only shows 68% capacity retention after 280 cycles. It is useful to note that the capacity retention capability of Si@OH/GO composite is comparable to the recently reported Si/graphene composite in the literature,[18−25] although this value is much lower than that of Si@NH_2/GO composite reported above. This result clearly demonstrates the importance and validity of dual chemical cross-linking/hydrogen bonding interactions between Si@NH_2 and GO, and between GO and binder. In addition, the electrochemical performance of the pristine Si NPs was also investigated under the same electrochemical test conditions for comparison. As illustrated in Figure 4c, the pristine Si NPs exhibit an initial charge capacity of 2471 mAh g^{-1}; however, the capacity decreases dramatically to 665 mAh g^{-1} after 150 cycles. This would be attributed to the poor intrinsic electronic conductivity and large volume change during Li insertion/extraction, leading to a loss of electrical contact between the active materials and the current collector. This result is also expected from the large resistance of the pristine Si NPs electrode (as shown in Figure S4 in the Supporting Information). In addition, the specific capacity and the cycle performance of Si@OH and Si@NH_2 were tested using the electrolyte without adding the VC (shown in Figure S5 in the Supporting Information). In comparison with the pristine Si@OH NPs, the Si@NH_2 material exhibits better cycle performance, with a specific charge capacity of 2530 mAh g^{-1} in the first cycle and 28.9% capacity retention after 50 cycles.

Figure 4d shows the rate performance of the Si@NH_2/GO and Si@OH/GO composites. For Si@NH_2/GO composite electrode, it delivers specific discharge capacities of 1100, 960, 760, 510, and 300 mAh g^{-1} at current densities of 210, 420, 840, 2100, and 4200 mA g^{-1}, respectively. When the current density is decreased from 4200 mA g^{-1} to 210 mA g^{-1}, the discharge capacity goes back up to 1120 mAh g^{-1}, revealing the superior reversibility of Si@NH_2/GO and its suitability as an anode material with good rate performance. This again demonstrates that the dual chemical cross-linking/hydrogen bonding interactions architecture of the material is tolerant to various charge and discharge currents, which is a characteristic required for high-powered applications. Although the Si@OH/GO composite electrode shows similar discharge capacity to the Si@NH_2/GO composite electrode at the same current densities, it cannot recover to its original value when the discharge current density resumes its original value after several cycles. This result shows that the Si@OH/GO composite[18−25] cannot act as a stable anode material at high rate. It is noted that the APTES molecules, which have been successfully grafted onto the surface of Si@OH NPs, play an important role in the excellent cycling and good rate performance of the Si@NH_2/GO composite, because they function as a buffer layer alleviating the effect of volume change during the insertion/extraction of lithium ions and also provide a positively charged surface to realize the self-assembling of Si with the negatively charged GO by chemical interactions.

To further understand the good cyclic and rate performance of the Si@NH_2/GO composite electrode, the electrochemical resistance of the Si@NH_2/GO composite electrode was measured using electrochemical impedance spectroscopy (EIS). Figure 5 displays the Nyquist plots of the half cell

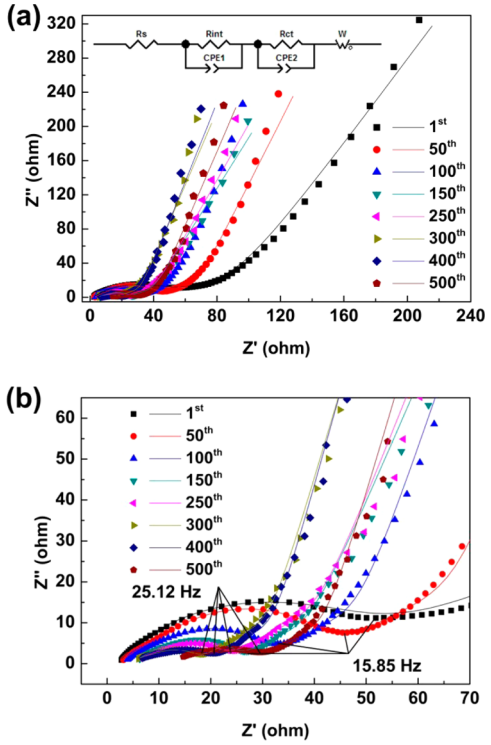

Figure 5. (a) Nyquist plots of the Si@NH_2/GO composite anode after a series of cycles at 420 mA g^{-1} and (b) close-up of Nyquist plots of the Si@NH_2/GO composite anode after a series of cycles at 420 mA g^{-1}. The symbols represent the EIS measurement data, and the lines are fitting curves using the equivalent circuit.

with the composite working electrode after different charged cycles. EIS measurements were performed after 1, 50, 100, 150, 250, 300, 400, and 500 cycles under the cycling rate of 420 mA g^{-1}. The internal impedance of the cell can be described by its equivalent circuit, which is also plotted as the inset of Figure 5a. In the equivalent circuit, R_s is the resistance associated with the cell components, such as the electrolyte, the working electrode

(Si@NH_2/GO), and the counter electrode (Li foil). R_{int} is the interface resistance relevant to the SEI film, R_{ct} is the charge-transfer resistance for the electrode reaction, and W is the Warburg contribution, which is related to Li-ion diffusion into the Si@NH_2/GO.[14,51] The obtained impedances can be well-fitted with the equivalent circuit. The total impedance decreases initially, and then slowly increases after the 400th cycle. (Detailed results are listed in Table S1 in the Supporting Information.) The decrease in the impedances for the first few cycles may be attributed to two major reasons: the slow wetting of electrolyte into porous electrode, and the conductivity increase of Si nanoparticles after lithium-ion doping associated with electrochemical charging.[49] The improved reaction kinetics during the initial charge/discharge cycles resulted in a gradual increase in initial capacity (see Figure 4d). After 400 cycles, the capacity of the Si@NH_2/GO composite electrode slowly decreased (as shown in Figure S4 in the Supporting Information), corresponding to the increase in impedances (especially the quick increase in R_s). The possible reason for the quick increase in R_s is the deterioration of the counter electrode (Li anode). In contrast, both R_{int} and R_{ct} impedances of Si@OH/GO composite electrode (as shown in Figure S6 in the Supporting Information) increase after the first cycle, which indicates the continuous growth of the SEI during cycling.[49] The R_{int} (as listed in Table S1 in the Supporting Information) of the composite obviously increases after the first cycle, indicating that the SEI formed in the first cycle cannot withstand the strain/stress caused by lithium-ion intercalation in the following several cycles, resulting in rapid capacity loss and new SEI formation in the initial cycles. From the EIS data, one can be convinced that Si@NH_2/GO composite electrode is more resistant to mechanical strain/stress during lithium-ion insertion/desertion than the Si@OH/GO composite electrode.

CONCLUSION

In summary, we developed a facile and scalable route to fabricate a novel Si@NH_2/GO-based electrode with high cycling stability by dual chemical cross-linking/hydrogen bonding interactions between surface-modified Si NPs and GO, and between GO and binder. The good mechanical flexibility, fast ionic and electronic transfer capability, and the number of function groups of GO play important roles. The dual chemical cross-linking/hydrogen bonding interactions between the functional buffer layer (APTES) and GO, and between GO and binder provided three stable interfaces—between Si NPs and APTES, between APTES and GO, and between GO and binder—to enhance the cycling performance of Si-based anodes. The obtained Si@NH_2/GO compound exhibited excellent cycling performance with specific reversible capacity up to 1000 mAh g^{-1} at a current density of 420 mA g^{-1} after 400 cycles. Its rate performance is also shown to be good. The great improvement of cyclic performance achieved in this anode is attributed to the use of APTES buffer layer, GO, and Salg, which effectively integrate the Si NPs, GO and binder into a stable electrode. This strategy for designing a durable Si-based electrode at a systematic level could be extended to other high-capacity electrode materials to achieve improved cycling performance.

ASSOCIATED CONTENT

Supporting Information

The Raman spectra of different Si-based materials (Figure S1), the TG curves of GO, Si@OH/GO and Si@NH_2/GO (Figure S2), the discharge and charge profiles of GO at first cycle (Figure S3), the EIS results of Si (Figure S4), the cyclic performance of Si@OH and Si@NH_2 composites (Figure S5), the EIS spectra of Si@OH/GO (Figure S6), the SEM image of the cycled electrode (Figure S7), and the EIS fitting data of Si, Si@OH/GO (Table S1) are supplied as Supporting Information. This material is available free of charge via the Internet at http://pubs.acs.org.

AUTHOR INFORMATION

Corresponding Authors

*E-mail: chyfdeng@scut.edu.cn (Y. Deng).
*E-mail: kechengh@ust.hk (G. Chen).

Notes

The authors declare no competing financial interest.

ACKNOWLEDGMENTS

This work was supported by the Special Financial Grant from the China postdoctoral Science Foundation (No. 2013T60795), the Guangzhou Scientific and Technological Planning Projects (Nos. 2013J4100112 and 2014J4500002), the Fundamental Research Funds for the Central Universities (No. SCUT2012ZZ0042), and the Fok Ying Tung Foundation (No. NRC07/08.EG01).

REFERENCES

(1) Armand, M.; Tarascon, J. M. Building Better Batteries. *Nature* **2008**, *451*, 652−657.
(2) Goodenough, J. B.; Kim, Y. Challenges for Rechargeable Li Batteries. *Chem. Mater.* **2010**, *22*, 587−603.
(3) Chu, S.; Majumdar, A. Opportunities and Challenges for a Sustainable Energy Future. *Nature* **2012**, *488*, 294−303.
(4) Ji, L. W.; Lin, Z.; Alcoutlabi, M.; Zhang, X. W. Recent Developments in Nanostructured Anode Materials for Rechargeable Lithium-Ion Batteries. *Energy Environ. Sci.* **2011**, *4*, 2628−2699.
(5) Li, H.; Huang, X. J.; Chen, L. Q.; Wu, Z. G.; Liang, Y. A High Capacity Nano-Si Composite Anode Material for Lithium Rechargeable Batteries. *Electrochem. Solid-State lett.* **1999**, *2*, 547−549.
(6) Hatchard, T. D.; Dahn, J. R. J. In situ XRD and Electrochemical Study of the Reaction of Lithium with Amorphous Silicon. *J. Electrochem. Soc.* **2004**, *151*, A838−842.
(7) Kim, H.; Seo, M.; Park, M. H.; Cho, J. A Critical Size of Silicon Nano-Anodes for Lithium Rechargeable Batteries. *Angew. Chem., Int. Ed.* **2010**, *49*, 2146−2149.
(8) Yu, Y.; Gu, L.; Zhu, C.; Tsukimoto, S.; van Aken, P. A.; Maier, J. Reversible Storage of Lithium in Silver-Coated Three-Dimensional Macroporous Silicon. *Adv. Mater.* **2010**, *22*, 2247−2250.
(9) Chan, C. K.; Peng, H. L.; Liu, G.; McIlwrath, K.; Zhang, X. F.; Huggins, R. A.; Cui, Y. High-Performance Lithium Battery Anodes Using Silicon Nanowires. *Nat. Nanotechnol.* **2008**, *3*, 31−35.
(10) Park, M. H.; Kim, M. G.; Joo, J.; Kim, K.; Kim, J.; Ahn, S.; Cui, Y.; Cho, J. High-Performance Lithium Battery Anodes Using Silicon Nanowires. *Nano Lett.* **2009**, *9*, 3844−3847.
(11) Chen, D. Y.; Mei, X.; Ji, G.; Lu, M. H.; Xie, J. P.; Lu, J. M.; Lee, J. Y. Reversible Lithium-Ion Storage in Silver-Treated Nanoscale Hollow Porous Silicon Particles. *Angew. Chem., Int. Ed.* **2012**, *51*, 2409−2413.
(12) Cui, L. F.; Yang, Y.; Hsu, C. M.; Cui, Y. Carbon-Silicon Core-Shell Nanowires as High Capacity Electrode for Lithium Ion Batteries. *Nano Lett.* **2009**, *9*, 3370−3374.
(13) Liu, N.; Huo, K. F.; McDowell, M. T.; Zhao, J.; Cui, Y. Rice Husks as a Sustainable Source of Nanostructured Silicon for High Performance Li-Ion Battery Anodes. *Sci. Rep.* **2013**, *3*, 1919.
(14) Guo, J. C.; Chen, X. L.; Wang, C. S. Carbon Scaffold Structured Silicon Anodes for Lithium-Ion Batteries. *J. Mater. Chem.* **2010**, *20*, 5035−5040.

(15) Han, Z. J.; Yabuuchi, N.; Shimomura, K.; Murase, M.; Yui, H.; Komaba, S. High-Capacity Si-Graphite Composite Electrodes with a Self-formed Porous Structure by a Partially Neutralized Polyacrylate for Li-Ion Batteries. *Energy Environ. Sci.* **2012**, *5*, 9014−9020.
(16) Bhandavat, R.; Singh, G. Stable and Efficient Li-Ion Battery Anodes Prepared from Polymer-Derived Silicon Oxycarbide-Carbon Nanotube Shell/Core Composites. *J. Phys. Chem. C* **2013**, *117*, 11899−11905.
(17) Wang, W.; Kumta, P. N. Nanostructured Hybrid Silicon/Carbon Nanotube Heterostructures: Reversible High-Capacity Lithium-Ion Anodes. *ACS Nano* **2010**, *4*, 2233−2241.
(18) Zhou, X. S.; Yin, Y. X.; Wan, L. J.; Guo, Y. G. Facile Synthesis of Silicon Nanoparticles Inserted into Graphene Sheets as Improved Anode Materials for Lithium-Ion Batteries. *Chem. Commun.* **2012**, *48*, 2198−2200.
(19) Zhou, X. S.; Yin, Y. X.; Wan, L. J.; Guo, Y. G. Self-Assembled Nanocomposite of Silicon Nanoparticles Encapsulated in Graphene Through Electrostatic Attraction for Lithium-Ion Batteries. *Adv. Energy Mater.* **2012**, *2*, 1086−1090.
(20) Zhu, Y. H.; Liu, W.; Zhang, X. Y.; He, J. C.; Chen, J. T.; Wang, Y. P. Directing Silicon-Graphene Self-Assembly as a Core/Shell Anode for High-Performance Lithium-Ion Batteries. *Langmuir* **2013**, *29*, 744−749.
(21) Zhou, M.; Cai, T. W.; Pu, F.; Chen, H.; Wang, Z.; Zhang, H. Y.; Guan, S. Y. Graphene/Carbon-Coated Si Nanoparticle Hybrids as High-Performance Anode Materials for Li-Ion Batteries. *ACS Appl. Mater. Interfaces* **2013**, *5*, 3449−3455.
(22) Zhao, G. Y.; Zhang, L.; Meng, Y. F.; Zhang, N. Q.; Sun, K. N. Decoration of Graphene with Silicon Nanoparticles by Covalent Immobilization for Use as Anodes in High Stability Lithium Ion Batteries. *J. Power Sources* **2013**, *240*, 212−218.
(23) Park, S. H.; Kim, H. K.; Ahn, D. J.; Lee, S. I.; Roh, K. C.; Kim, K. B. Self-Assembly of Si Entrapped Graphene Architecture for High-Performance Li-Ion Batteries. *Electrochem. Commun.* **2013**, *34*, 117−120.
(24) Zhou, M.; Pu, F.; Wang, Z.; Cai, T. W.; Chen, H.; Zhang, H. Y.; Guan, S. Y. Facile Synthesis of Novel Si Nanoparticles−Graphene Composites as High-Performance Anode Materials for Li-Ion Batteries. *Phys. Chem. Chem. Phys.* **2013**, *15*, 11394−11401.
(25) Wen, Y.; Zhu, Y. J.; Langrock, A.; Manivannan, A.; Ehrman, S. H.; Wang, C. S. Graphene-Bonded and-Encapsulated Si Nanoparticles for Lithium Ion Battery Anodes. *Small* **2013**, *9*, 2810−2816.
(26) Chang, J. B.; Huang, X. K.; Zhou, G. H.; Cui, S. M.; Hallac, P. B.; Jiang, J. W.; Hurley, P. T.; Chen, J. H. Multilayered Si Nanoparticle/Reduced Graphene Oxide Hybrid as a High-Performance Lithium-Ion Battery Anode. *Adv. Mater.* **2014**, *26*, 758−764.
(27) Magasinski, A.; Zdyrko, B.; Kovalenko, I.; Hertzberg, B.; Burtovyy, R.; Huebner, C. F.; Fuller, T. F.; Luzinov, I.; Yushin, G. Toward Efficient Binders for Li-Ion Battery Si-Based Anodes: Polyacrylic Acid. *ACS Appl. Mater. Interfaces* **2010**, *2*, 3004−3010.
(28) Bridel, J. S.; Azaïs, T.; Morcrette, M.; Tarascon, J. M.; Larcher, D. Key Parameters Governing the Reversibility of Si/Carbon/CMC Electrodes for Li-Ion Batteries. *Chem. Mater.* **2010**, *22*, 1229−1241.
(29) Du, C. Y.; Gao, C. H.; Yin, G. P.; Chen, M.; Wang, L. Facile Fabrication of a Nanoporous Silicon Electrode with Superior Stability for Lithium Ion Batteries. *Energy Environ. Sci.* **2011**, *4*, 1037−1042.
(30) Kovalenko, I.; Zdyrko, B.; Magasinski, A.; Hertzberg, B.; Milicev, Z.; Burtovyy, R.; Luzinov, I.; Yushin, G. A Major Constituent of Brown Algae for Use in High-Capacity Li-Ion Batteries. *Science* **2011**, *334*, 75−79.
(31) Koo, B.; Kim, H.; Cho, Y.; Lee, K. T.; Choi, N. S.; Cho, J. A Highly Cross-Linked Polymeric Binder for High-Performance Silicon Negative Electrodes in Lithium Ion Batteries. *Angew. Chem., Int. Ed.* **2012**, *51*, 8762−8767.
(32) Ryou, M. H.; Kim, J.; Lee, I.; Kim, S.; Jeong, Y. K.; Hong, S.; Ryu, J. H.; Kim, T. S.; Park, J. K.; Lee, H.; Choi, J. W. Mussel-Inspired Adhesive Binders for High-Performance Silicon Nanoparticle Anodes in Lithium-Ion Batteries. *Adv. Mater.* **2013**, *25*, 1571−1576.
(33) Acres, R. G.; Ellis, A. V.; Alvino, J.; Lenahan, C. E.; Khodakov, D. A.; Metha, G. F.; Andersson, G. G. Molecular Structure of 3-Aminopropyltriethoxysilane Layers Formed on Silanol-Terminated Silicon Surfaces. *J. Phys. Chem. C* **2012**, *116*, 6289−6297.
(34) Xu, W. J.; Riikonen, J.; Nisssnen, T.; Suvanto, M.; Rilla, K.; Li, B.; Wang, Q.; Deng, F.; Lehto, V. P. Amine Surface Modifications and Fluorescent Labeling of Thermally Stabilized Mesoporous Silicon Nanoparticles. *J. Phys. Chem. C* **2012**, *116*, 22307−22314.
(35) Li, D.; Muller, M. B.; Cilje, S.; Kaner, R. B.; Wallace, G. G. Processable Aqueous Dispersions of Graphene Nanosheets. *Nat. Nanotechnol.* **2008**, *3*, 101−105.
(36) Ji, L. W.; Rao, M. M.; Zheng, H. M.; Zhang, L.; Li, Y. C.; Duan, W. H.; Guo, J. H.; Cairns, E. J.; Zhang, Y. G. Graphene Oxide as a Sulfur Immobilizer in High Performance Lithium/Sulfur Cells. *J. Am. Chem. Soc.* **2011**, *133*, 18522−18525.
(37) Hummers, W. S.; Offeman, R. E. Preparation of Graphitic Oxide. *J. Am. Chem. Soc.* **1958**, *80*, 1339−1339.
(38) Kovtyukhova, N. I.; Ollivier, P. J.; Martin, B. R.; Mallouk, T. E.; Chizhik, S. A.; Buzaneva, E. V.; Gorchinskiy, A. D. Layer-by-Layer Assembly of Ultrathin Composite Flms from Micron-Sized Graphite Oxide Sheets and Polycations. *Chem. Mater.* **1999**, *11*, 771−778.
(39) Wang, L.; Wang, D.; Dong, Z. H.; Zhang, F. X.; Jin, J. Interface Chemistry Engineering for Stable Cycling of Reduced GO/SnO_2 Nanocomposites for Lithium Ion Battery. *Nano Lett.* **2013**, *13*, 1711−1716.
(40) Hiyoshi, N.; Yogo, K.; Yashima, T. Adsorption Characteristics of Carbon Dioxide on Organically Functionalized SBA-15. *Microporous Mesoporous Mater.* **2005**, *84*, 357−365.
(41) Sreejith, S.; Ma, X.; Zhao, Y. L. Graphene Oxide Wrapping on Squaraine-Loaded Mesoporous Silica Nanoparticles for Bioimaging. *J. Am. Chem. Soc.* **2012**, *134*, 17346−17349.
(42) Ferrari, A. C.; Meyer, J. C.; Scardaci, V.; Casiraghi, C.; Lazzeri, M.; Mauri, F.; Piscanec, S.; Jiang, D.; Novoselov, K. S.; Roth, S.; Geim, A. K. Raman Spectrum of Graphene and Graphene Layers. *Phys. Rev. Lett.* **2006**, *97*, 187401−187404.
(43) Briggs, D.; Seah, M. P. *Practical Surface Analysis*, 2nd Edition; Wiley: Chichester, U.K., New York, 1990; Vol. *1*.
(44) Wang, L.; Wang, D.; Dong, X.; Zhang, Z.; Pei, X.; Chen, X.; Chen, B.; Jin, J. Layered Assembly of Graphene Oxide and Co-Al Layered Double Hydroxide Nanosheets as Electrode Materials for Supercapacitors. *Chem. Commun.* **2011**, *47*, 3556−3558.
(45) Vandenberg, E. T.; Bertilsson, L.; Liedberg, B.; Uvdal, K.; Erlandsson, R.; Elwing, H.; Lundström, I. Structure of 3-Aminopropyl Triethoxy Silane on Silicon Oxide. *J. Colloid Interface Sci.* **1991**, *147*, 103−118.
(46) Yang, S. B.; Feng, X. L.; Wang, X. C.; Müllen, K. Graphene-Based Carbon Nitride Nanosheets as Efficient Metal-Free Electrocatalysts for Oxygen Reduction Reactions. *Angew. Chem., Int. Ed.* **2011**, *50*, 5339−5343.
(47) Profatilova, I. A.; Stock, C.; Schmitz, A.; Passerini, S.; Winter, M. Enhanced Thermal Stability of a Lithiated Nano-Silicon Electrode by Fluoroethylene Carbonate and Vinylene Carbonate. *J. Power. Sources* **2013**, *222*, 140−149.
(48) Lee, H. H.; Wang, Y. Y.; Wan, C. C.; Yang, M. H.; Wu, H. C.; Shieh, D. T. The Function of Vinylene Carbonate as a Thermal Additive to Electrolyte in Lithium Batteries. *J. Appl. Electrochem.* **2005**, *35*, 615−623.
(49) Wu, H.; Yu, G. H.; Pan, L. J.; Liu, N.; McDowell, M. T.; Bao, Z. N.; Cui, Y. Stable Li-ion Battery Anodes by in-situ Polymerization of Conducting Hydrogel to Conformally Coat Silicon Nanoparticles. *Nat. Commun.* **2013**, *4*, 1943−1948.
(50) Li, L.; Raji, A. R. O.; Tour, J. M. Graphene-Wrapped MnO_2−Graphene Nanoribbons as Anode Materials for High-Performance Lithium Ion Batteries. *Adv. Mater.* **2013**, *25*, 6298−6302.
(51) Yu, P.; Haran, B. S.; Ritter, J. A.; White, R. E.; Popov, B. N. Palladium-Microencapsulated Graphite as the Negative Electrode in Li-Ion Cells. *J. Power Sources* **2000**, *91*, 107−117.